ISSN 1063-7710, Acoustical Physics, 2019, Vol. 65, No. 1, pp. 7–13. © Pleiades Publishing, Ltd., 2019.

CLASSICAL PROBLEMS OF LINEAR ACOUSTICS AND WAVE THEORY

Acoustic Scattering from a Cylindrical Shell with Double Internal Rigid Plates[1]

Yunzhe Tong[a], Wang Wei[a], Jun Fan[a, *], and Bin Wang[a]

[a]*Collaborative Innovation Center for Advanced Ship and Deep-Sea Exploration, State Key Laboratory of, Ocean Engineering, Shanghai Jiao Tong University, Shanghai, 200240 China*

**e-mail:fanjun@sjtu.edu.cn*

Received March 9, 2018; Revised June 4, 2018; Accepted August 28, 2018

Abstract—The acoustic scattering from an infinite cylindrical shell with double internal rigid plates at normal incidence is studied by theoretical and experimental approaches. The two rigid plates are attached to the shell along lines parallel to the shell axis symmetrically. The dominant feature of frequency-angle spectra is the interference fringes caused by the reflection waves of attachments in the illuminated region and specular reflection. For a cylindrical shell with double internal plates, there may be several attachments in the illuminated region simultaneously. There will be bright spots when two interference fringes caused by two attachments in the illuminated region intersect, while only interference fringes can be observed for one attachment in the illuminated region. Theoretical and experimental results show that the number of attachments in illuminated region can significantly affect the scattering characteristics, and it is a prominent feature to identify the location of internal plates.

Keywords: acoustic scattering, cylindrical shell, lengthwise stiffeners

DOI: 10.1134/S1063771019010123

1. INTRODUCTION

Underwater vehicles play an irreplaceable role in ocean resource exploration and protection. Since most of the underwater vehicles can be approximated as cylindrical shells with internal stiffeners, the study of the acoustic scattering characteristics of stiffened cylindrical shell has become very popular. The internal stiffeners can be separated into linear circumferential stiffeners and linear lengthwise stiffeners, and the internal longitudinal plate is a typical kind of lengthwise stiffener.

Early studies of lengthwise stiffener showed that lengthwise ribs can cause the transformations of circumferential waves from one type to another at the attachment of the lengthwise ribs to the cylindrical shell [1–5]. In practice, internal longitudinal plates are often used in underwater vehicles. Most studies of the acoustic scattering characteristics of the cylindrical shell with internal longitudinal plate are focused on the normal incidence [6–10]. Previous works have indicated that the dominant acoustic scattering characteristics are caused by the geometrical configuration and the shell properties [6]. Tyutekin et al. studied the acoustic scattering from an elastic cylindrical shell with longitudinal rigid fixations [8, 9]. Skelton derived formulae of the acoustic scattering field from an infinitely long cylindrical shell with two internal longitudinal rigid plates, in which dynamics of the internal plates are neglected [11]. Later, based on the quantitative ray analysis [12], Tong et al. analyzed the scattering mechanism of a cylindrical shell with an internal rigid plate through theory and experiment [10]. The dominant features in backscattered pressure from a cylindrical shell with an internal rigid plate can be explained by the resonance of the shell and the interference between the reflection waves and re-radiation waves. However, the scattering mechanism of a cylindrical shell with double internal rigid plates which exists more commonly in practical underwater vehicles remains to be studied.

Currently, with the development of computer, the vibration and scattering of inhomogeneous shells can be calculated numerically [13, 14]. However, to analyze the scattering mechanism of a cylindrical shell with double internal rigid plates in depth, the analytical method is used in this paper.

This paper is organized as follows: Presented in Sec. 2 is the theoretical background of acoustic backscattering from a cylindrical shell with double internal rigid plates at normal incidence. The two internal plates are located in the cylindrical shell symmetrically. Afterwards, in Sec. 3, numerical simulation results are presented as frequency-angle spectra of the backscattered pressure form function, and the influ-

[1] The article is published in the original.

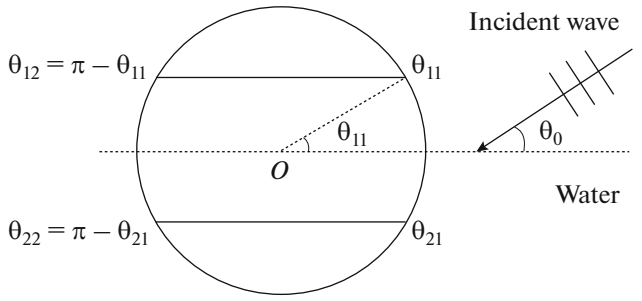

Fig. 1. Geometry of a cylindrical shell with double internal rigid plates.

ence of the attachments of plates to cylindrical shell is analyzed. The experimental setup and model used to validate the theory are presented in Sec. 4. Experimental and theoretical frequency-angle spectra of the backscattered sound field are compared and the interference phenomenon in the experimental result is in a good agreement with that in the theoretical result. Finally, a brief summary and conclusions are presented in Sec. 5.

2. THEORETICAL BACKGROUND

Consider that a vacuumed cylindrical shell of radius a, thickness h_s, Young's modulus E_s, Poisson's ratio σ_s, and density ρ_s, is loaded with two rigid plates and submerged in an acoustic medium of density ρ_f and sound velocity c_f. A polar coordinate system (r,θ) is used to describe the two-dimensional problem. The origin "O" of the polar coordinate system is at the center of the shell, as shown in Fig. 1. The incident acoustic plane wave can be specified as

$$p_{\text{inc}}(r,\theta) = \sum_{n=-\infty}^{+\infty} (-i)^n J_n(k_f r) e^{in(\theta-\theta_0)}. \tag{1}$$

The time-harmonic factor $e^{-i\omega t}$ is suppressed. θ_0 is the incident angle, $k_f = \omega/c_f$ is the exterior fluid acoustic wavenumber, and J_n is the Bessel function of the first kind of order n. The scattering pressure p_{scat} satisfies the reduced wave equation that permits solutions of the form:

$$p_{\text{scat}}(r,\theta) = \sum_{n=-\infty}^{+\infty} C_n H_n(k_f r) e^{in(\theta-\theta_0)}, \tag{2}$$

where H_n is the n-th order Hankel function of the first kind, C_n are the unknown coefficients, which will be determined by solving the displacements of the shell as well as the coupling between the incident wave and the shell. It is a two-dimensional problem for the acoustic scattering from an infinite cylindrical shell at normal incidence. Neglecting the axial displacement of the shell, the motions of the shell are described by the Donnell equation as follows:

$$\begin{cases} \left(k_s^2 a^2 - 1\right) u_r - \dfrac{\partial u_\theta}{\partial \theta} - \dfrac{h_s^2}{12a^2}\dfrac{\partial^4 u_r}{\partial \theta^4} \\ = 2\pi\mu\left(a p_{\text{scat}} + a p_{\text{inc}} - q_r\right), \\ k_s^2 a^2 u_\theta + \dfrac{\partial^2 u_\theta}{\partial \theta^2} + \dfrac{\partial u_r}{\partial \theta} = -2\pi\mu q_\theta, \end{cases} \tag{3}$$

where u_r and u_θ are the radial and circumferential displacements of the loaded cylindrical shell, $k_s = \omega/c_s$ with $c_s^2 = E_s/\rho_s\left(1-\sigma_s^2\right)$, and μ, q_r, q_θ are introduced to save writing:

$$\mu = a/2\pi c_s^2 \rho_s h_s, \tag{4}$$

$$\begin{cases} q_r = \sum_{i=1}^{2}\sum_{j=1}^{2} F_r^{(ij)} \delta(\theta - \theta_{ij}), \\ q_\theta = \sum_{i=1}^{2}\sum_{j=1}^{2} F_\theta^{(ij)} \delta(\theta - \theta_{ij}). \end{cases} \tag{5}$$

The analytical solutions of Eq. (3) for the radial and circumferential displacements of the shell can be expressed as follows:

$$\begin{cases} u_r(\theta) = \sum_{n=-\infty}^{+\infty} U_n e^{in\theta} \\ u_\theta(\theta) = \sum_{n=-\infty}^{+\infty} V_n e^{in\theta} \end{cases}. \tag{6}$$

The total pressure $p_{\text{inc}} + p_{\text{scat}}$ in the fluid must satisfy the boundary condition at the shell interfaces:

$$-\rho_f \omega^2 u_r + \frac{\partial p_{\text{scat}}}{\partial r} + \frac{\partial p_{\text{inc}}}{\partial r} = 0. \tag{7}$$

By using the boundary condition, we can obtain:

$$C_n = \frac{\rho_f \omega^2 U_n - (-i)^n k_f J_n'(k_f a) e^{-in\theta_0}}{k_f H_n'(k_f a)}, \tag{8}$$

where the prime sign denotes differentiation with respect to the argument. Furthermore, u_r and u_θ can be expressed as follows:

$$u_r(\theta) = u_r^{(0)}(\theta) + \mu\sum_{i=1}^{2}\sum_{j=1}^{2}\left[F_r^{(ij)}\Lambda(\theta,\theta_{ij}) + F_\theta^{(ij)}\Gamma(\theta,\theta_{ij})\right], \tag{9}$$

$$u_\theta(\theta) = u_\theta^{(0)}(\theta) - \mu\sum_{i=1}^{2}\sum_{j=1}^{2}\left[F_r^{(ij)}\Gamma(\theta,\theta_{ij}) + F_\theta^{(ij)}\Pi(\theta,\theta_{ij})\right], \tag{10}$$

where $u_r^{(0)}$ and $u_\theta^{(0)}$ are the radial and circumferential displacements of the empty shell. $\Lambda(\theta,\theta_{ij})$, $\Gamma(\theta,\theta_{ij})$

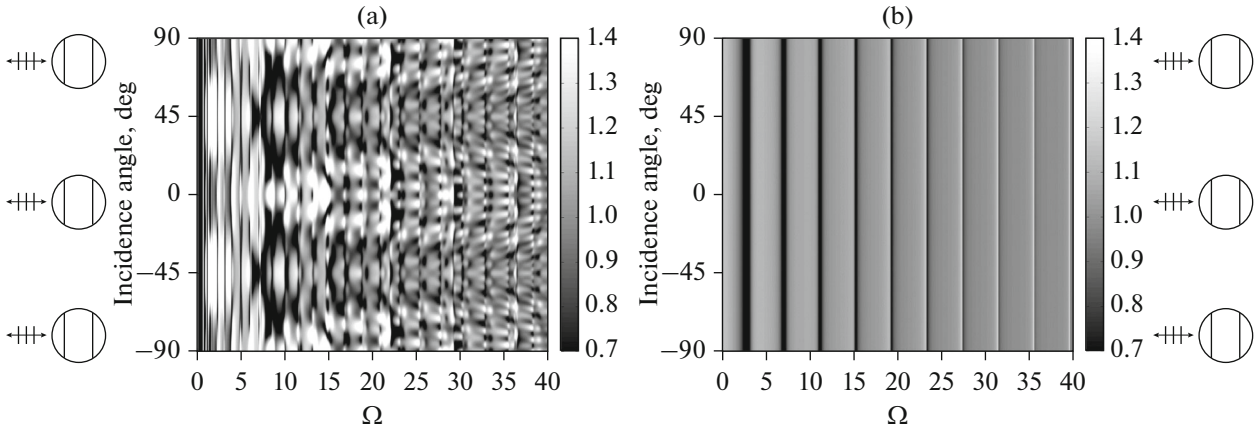

Fig. 2. Frequency-angle spectra of the backscattered pressure form function. (a) Loaded cylindrical shell, (b) empty cylindrical shell.

and $\Pi(\theta,\theta_{ij})$ are auxiliary functions described in the Appendix. By setting θ to θ_{11}, θ_{12}, θ_{21} and θ_{22} in $u_r(\theta)$ and $u_\theta(\theta)$, we obtain

$$\mathbf{U} = \mathbf{U}^{(0)} + \mu\mathbf{H}\mathbf{F}, \tag{11}$$

where

$$\mathbf{U} = \left[u_r(\theta_{11}),\ldots,u_\theta(\theta_{11}),\ldots\right]^{\mathrm{T}}, \tag{12}$$

$$\mathbf{F} = \left[F_r^{(11)}(\theta_{11}),\ldots,F_\theta^{(11)}(\theta_{11}),\ldots\right]^{\mathrm{T}}, \tag{13}$$

and $\mathbf{H}$ is a 8×8 matrix of the form

$$\mathbf{H} = \begin{pmatrix} \mathbf{\Lambda} & \mathbf{\Gamma} \\ -\mathbf{\Gamma} & -\mathbf{\Pi} \end{pmatrix}. \tag{14}$$

Each component in Eq. (14) is a 4×4 matrix. The dynamics of the internal plate can be neglected for the heavy internal plates [6]. In practical engineering applications, many equipments are deployed on the internal plates, which means the internal plates are generally very heavy, so that we can regard the internal plates as rigid. Hence, at the junction of the cylindrical shell and plates, the only possible rigid body motion is zero motion:

$$\mathbf{U} = \mathbf{U}^{(0)} + \mu\mathbf{H}\mathbf{F} = 0, \tag{15}$$

and the reaction force matrix can be obtained:

$$\mathbf{F} = -(\mu\mathbf{H})^{-1}\mathbf{U}^{(0)}. \tag{16}$$

Now, having found $\mathbf{F}$, the coefficients C_n can be derived from Eqs. (8) and (9), so that the scattered pressure p_{scat} can be obtained. The backscattered pressure form function $f(\Omega,\theta)$ defined by

$$p_{\mathrm{scat}}(\omega,r,\theta) = \sqrt{\frac{a}{2r}}e^{ik_f r} f(\Omega,\theta), \tag{17}$$

is introduced to measure the acoustic field, where $\Omega = \dfrac{\omega}{c_f}a$ and $r \to +\infty$. More details can be found in Ref. [6].

3. NUMERICAL APPLICATIONS

The parameters for numerical calculation and experiment are summarized in the Table 1. First, as illustrated in Fig. 2, the frequency–angle spectra of the backscattered pressure form function [defined by Eq. (17)] for a loaded cylindrical shell ($\theta_{11} = \pi/4$, $\theta_{21} = -\pi/4$) and an empty cylindrical shell is calculated for comparison. The horizontal coordinate is the normalized frequency Ω, and the vertical coordinate is the incidence angle θ_0.

Comparing Figs. 2a, 2b, when the cylindrical shell is loaded with double internal rigid plates, the frequency-angle spectra of the backscattered pressure form function becomes much more complex. The vertical lines in Fig. 2b are caused by the s_0-wave resonance. The resonance phenomenon of the empty cylindrical shell has been well studied previously [15–17]. For the calculated frequency, the s_0-wave is a supersonic wave, while the flexural wave is not. Thereby, when the wavelength λ_{s_0} of the s_0-wave satisfies $2\pi a = n\lambda_{s_0}$, the s_0-wave will form a standing wave in the circumferential waves, which leads to a resonance of their amplitudes and, hence, leads to acoustic scattering resonances [17]. This is also the dominant feature for the frequency-angle spectra of the backscattered pressure form function of the empty cylindrical shell at calculated frequency. The resonance of the s_0-wave can also be observed for the loaded cylindrical shell, but the acoustic features caused by the internal plates become dominant in the frequency-angle spectra of the backscattered pressure form function.

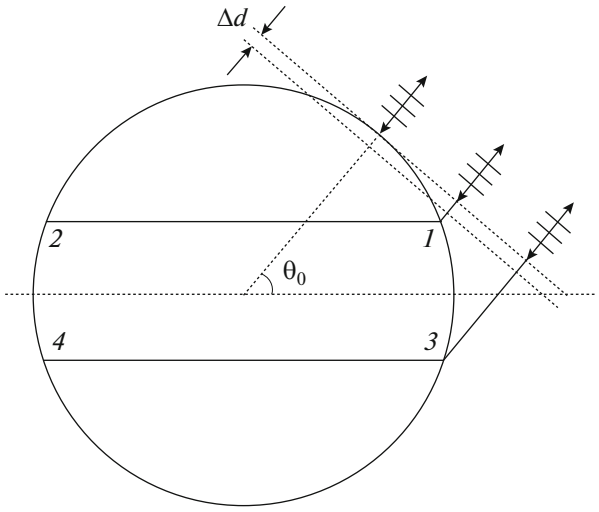

Fig. 3. Illustration of interference between specular reflection wave and geometric reflection wave from the attachment points.

From Fig. 2a it can be observed that there exists a lot of bright spots correlated to Ω and incidence angle θ_0. For the incidence angle of about 0° and $\pm 90^\circ$, the bright spots are intensive, while for the incidence angle of about $\pm 45^\circ$, the bright spots are spare. Since the dynamics of the internal plates is neglected, the acoustic features are caused by the geometrical configuration of the attachments and the shell properties.

For the cylindrical shell with circumferential stiffeners, the Bragg scattering is excited by the interference of the reflection waves from the periodic circumferential stiffeners. The attachments of internal plates to the shell can also reflect acoustic wave. However, these reflection waves from the attachments can not only interfere with each other, but also interfere with the specular reflection. The bright spots are caused by the constructive interference of the reflection wave and specular reflection. If more than one reflection waves interfere with the specular reflection, the interference phenomenon becomes much more complex. As the cylindrical shell with circumferential stiffeners, there also exists Bloch wave scattering in the cylindrical shell with lengthwise stiffeners [10]. The attachment in the illuminated region can generate and reradiate the flexural wave. However, there are many attachments in the illuminated region simultaneously, the reflection waves from the attachments make it difficult to distinguish the Bloch wave scattering. The energy of Bloch wave scattering is much weaker than that of reflection waves of the attachments, and the trajectory of Bloch wave scattering can be easily masked by that of reflection waves of the attachments in the backscattered pressure frequency–angle spectra. As a result, the phenomenon caused by the reflection waves of the attachments in the illuminated region will be mainly discussed in this paper.

As illustrated in Fig. 3, constructive interference occurs when the phase difference between the specular reflection wave and geometric reflection wave from the attachments is an even multiple of π. From the geometric relationship, a simple formula can be derived for predicting the constructive interference fringes:

$$\Omega = \frac{n\pi - \Delta\varphi}{1 - \cos(\theta_0 - \theta_{ij})}, \quad |\theta_0 - \theta_{ij}| < \frac{\pi}{2}, \quad n = 1,2\ldots, \quad i,j = 1,2. \tag{18}$$

Where $\Delta\varphi$ is the adjustment. Eq. (17) is obtained since the specular reflection wave can be approximated as the contribution from the first Fresnel half-zone. Considering the characteristic of the specular reflection wave and assuming the equivalent specular reflection point located at $\Delta d = \lambda/8$, the adjustment can be set to $\Delta\varphi = \pi/4$.

Figure 4 is the prediction for the interference fringes of the specular wave and reflection wave from attachments ($\theta_{11} = \pi/4$, $\theta_{21} = -\pi/4$) in the illuminated region. Figures 4a, 4b plot interference fringes caused by the interference between the specular wave and the reflection wave from different attachments, and the orders of attachments labeled in Fig. 4 are illustrated in Fig. 3. It can be observed that most of the bright spots exist at the interaction of these interference fringes. The interference between the specular reflection wave and reflection waves of attachments in the illuminated region is the dominant feature of the acoustic scattering from a cylindrical shell with double internal rigid plates.

4. EXPERIMENT

An air-filled cylindrical shell with double internal plates ($\theta_{11} = \pi/4$, $\theta_{21} = -\pi/4$) is made of stainless steel, with a thickness of 0.11 cm and a length of 60 cm. The two 0.2 cm-thick internal longitudinal plates soldered longitudinally along the shell are made of the same material as the shell. Other parameters are listed in the Table 1. The cylindrical shell closed by two flat endcaps is vertically immersed in a $5\times5\times5$ m water-filled tank. The tank is specially designed for studying the scattering mechanism of underwater acoustic. The photographs of the experimental model and tank are illustrated in Fig. 5.

The experimental model spins around its axe at a speed of $40^\circ/\text{min}$, which is controlled by a computer accurately. The transducer and receiver are fixed properly. Limited by the bandwidth of the transducer, the frequency range of the study extends over the range 60–120 kHz. The experimental setup is illustrated in Fig. 6. The entire measurement system is powered by a

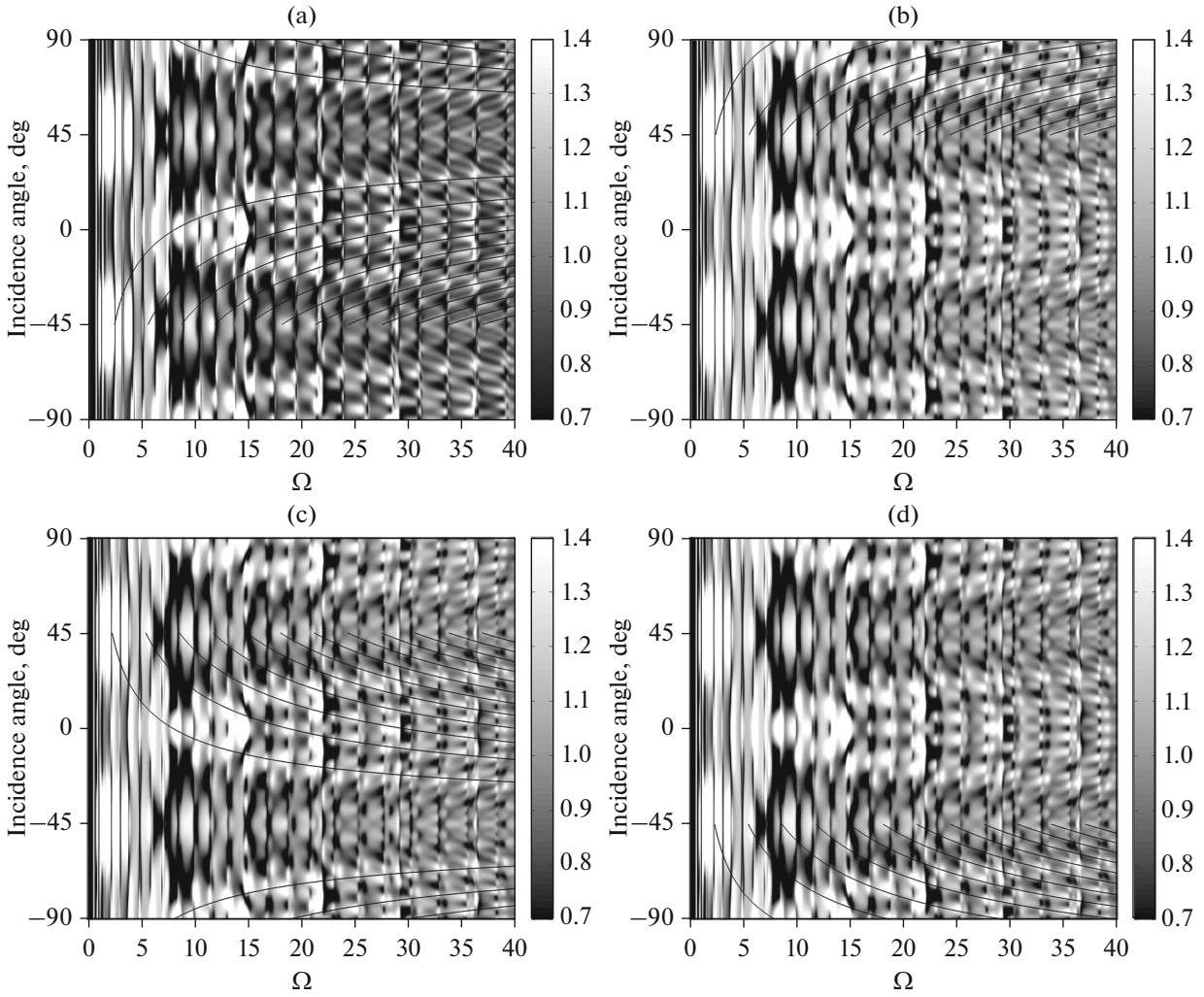

Fig. 4. Frequency-angle spectra of the backscattered pressure form function. Black curves show the interference fringes of the specular reflection with: (a) attachment 1, (b) attachment 2, (c) attachment 3, (d) attachment 4.

high-capacity uninterruptible power supply (UPS) to get rid of the power line interference.

A long chirp pulse (2.5 ms, 60–120 kHz) is projected to the experimental model from the transducer. Two pulses are projected each second. The sample frequency of the data acquisition system is 1 MHz. The direct signal is also recorded for spectra modification. The Fast Fourier Transform of NFFT = 8192 is used to process the signal. Figure 7 plots the comparison of experimental and theoretical results. The experimental steps are at 0.04 Ω. Due to the frequency response of the emitter and receiver transducer, the recorded signal is hard to match with the initial chirp.

It can be seen from Fig. 7 that the interference fringes between the specular reflection wave and attachment reflection wave agree well with prediction. As the experimental model is not completely symmetrical at the attachments, Fig. 7a is not symmetrical to 0°. Besides, the s_0-wave resonance is not clearly observed, since the experimental model is not slender enough and the experimental results are affected by the finite length of the experimental model. In the experimental results, intensive bright spots can be observed when the incident angle is near 0° and $\pm 90^{\circ}$, since there are two attachments in the illuminated

Table 1. Parameters of the shell and fluid

Shell	Radius	$a = 8$ cm
	Thickness	$h_s = 0.11$ cm
	Density	$\rho_s = 7850$ kg/m^3
	Young's modulus	$E_s = 2.1 \times 10^{11}$ Pa
Fluid	Longitudinal velocity	$c_f = 1500$ m/s
	Density	$\rho_f = 1000$ kg/m^3

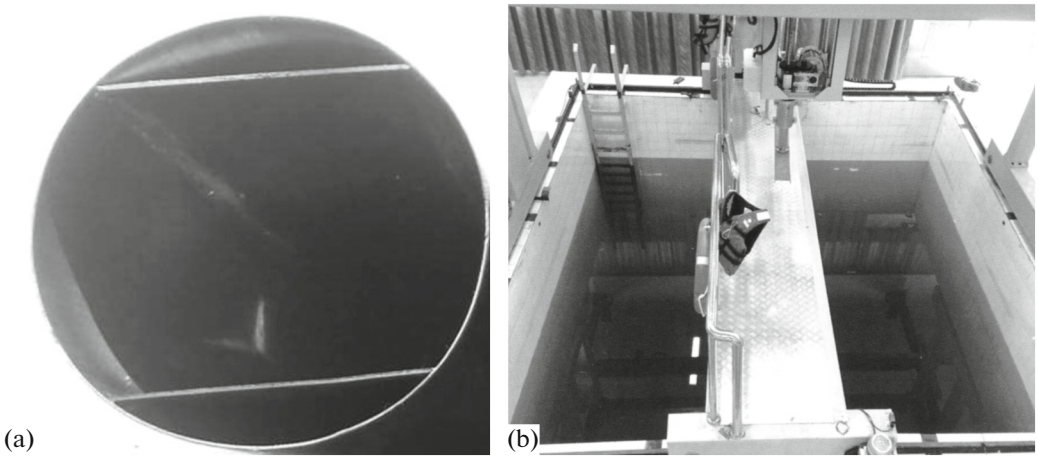

Fig. 5. Photographs of (a) the experimental model and (b) the water-filled tank.

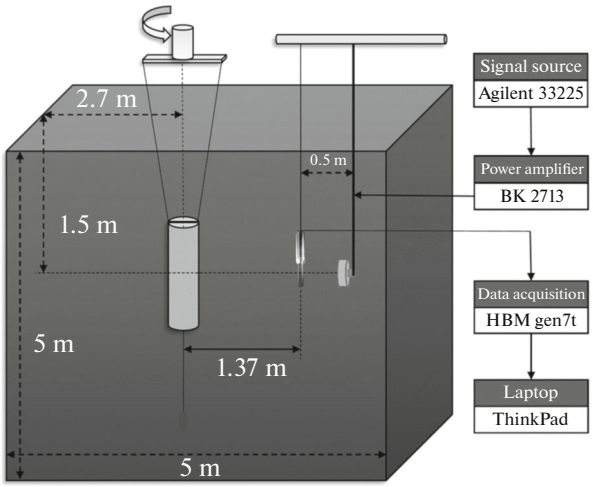

Fig. 6. Experimental setup.

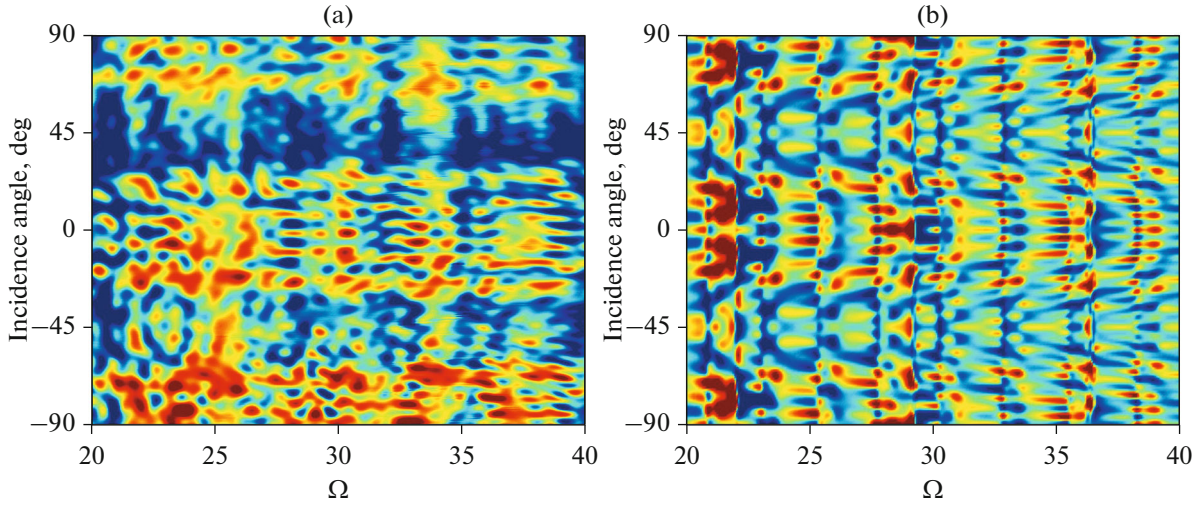

Fig. 7. Frequency-angle spectra of the backscattered pressure form function of the cylindrical shell with double internal rigid plates. (a) Experimental results, (b) calculated results.

region simultaneously. Complex interference phenomenon occurs when the incident angle is near 0° and $\pm 90^{\circ}$, which is a distinguishing feature to identify the location of the internal plates.

5. CONCLUSIONS

The scattering mechanisms of an immersed cylindrical shell with double internal rigid plates have been analyzed through numerical and experimental methods. The interference phenomenon caused by the specular reflection wave and attachments reflection waves are discussed in detail. Furthermore, a simple formula for predicting the interference features in the frequency-angle spectra is derived and the location of the symmetrical plates can be identified by the scattering features.

When the acoustic wave illuminates the cylindrical shell, besides the specular reflection, the attachments in the illuminated region can also reflect acoustic wave strongly. The specular reflection wave and attachments reflection waves can interfere with each other and induce interference fringes in the frequency–angle spectra. Moreover, if two attachments are in the illuminated region simultaneously, bright spots can be observed on the intersection of the interference fringes. The bright spots and interference fringes show dramatic difference in the frequency-angle spectra, so further work consists in identifying the location of the symmetrical plates by the scattering characteristics and a proper signal processing [18].

APPENDIX

The radial and circumferential components of the empty-shell displacement can be expressed as follows:

$$u_r^{(0)} = \sum_{n=-\infty}^{\infty} \frac{4\mu b_n a (-i)^n e^{in(\theta-\theta_0)}}{iD_n}, \quad \text{(A1)}$$

$$u_\theta^{(0)} = -\sum_{n=-\infty}^{\infty} \frac{4n\mu a (-i)^n e^{in(\theta-\theta_0)}}{D_n}. \quad \text{(A2)}$$

The auxiliary functions $\Lambda(\theta,\theta_{ij})$, $\Gamma(\theta,\theta_{ij})$ and $\Pi(\theta,\theta_{ij})$ can be expressed as follows:

$$\Lambda(\theta,\theta_{ij}) = \sum_{n=-\infty}^{\infty} \frac{b_n}{A_n} e^{in(\theta-\theta_{ij})}, \quad \text{(A3)}$$

$$\Gamma(\theta,\theta_{ij}) = \sum_{n=-\infty}^{\infty} \frac{in}{A_n} e^{in(\theta-\theta_{ij})}, \quad \text{(A4)}$$

$$\Pi(\theta,\theta_{ij}) = \sum_{n=-\infty}^{\infty} \frac{a_n}{A_n} e^{in(\theta-\theta_{ij})}. \quad \text{(A5)}$$

a_n and b_n are defined by

$$a_n = 1 - k_s^2 a^2 + \frac{h_s^2}{12a^2} n^4 + kaE_f \frac{H_n(k_f a)}{H_n'(k_f a)}, \quad \text{(A6)}$$

$$b_n = k_s^2 a^2 - n^2, \quad \text{(A7)}$$

where $E_f = c_f^2 \rho_f a / c_s^2 \rho_s h_s$ and

$$A_n = a_n b_n + n^2, \quad \text{(A8)}$$

$$D_n = k_f a H_n'(k_f a) A_n. \quad \text{(A9)}$$

ACKNOWLEDGMENTS

We wish to acknowledge the support of the National Science Foundation for a Distinguished Young Scholars of China Grant (no. 11504233). We would like to thank Prof. Weilin Tang and Dr. Zilong Peng for many discussions on simulations and valuable comments.

REFERENCES

1. A. Klauson and J. Metsaveer, J. Acoust. Soc. Am. **91** (4), 1834 (1992).
2. A. Klauson, G. Maze, and J. Metsaveer, J. Acoust. Soc. Am. **96** (3), 1575 (1994).
3. A. Klauson, J. Metsaveer, D. Decultot, G. Maze, and J. Ripoche, J. Acoust. Soc. Am. **100** (5), 3135 (1996).
4. J. Chiumia, N. Touraine, D. Decultot, G. Maze, A. Klauson, and J. Metsaveer, J. Acoust. Soc. Am. **105** (1), 183 (1999).
5. A. Baillard, J. Chiumia, D. Decultot, G. Maze, A. Klauson, and J. Metsaveer, J. Acoust. Soc. Am. **124** (4), 2061 (2008).
6. Y. P. Guo, J. Acoust. Soc. Am. **93** (4), 1936 (1993).
7. A. Baillard, J. M. Conoir, D. Decultot, G. Maze, A. Klauson, and J. Metsaveer, J. Acoust. Soc. Am. **107** (4), 3208 (2000).
8. V. V. Tyutekin, A. I. Boiko, and Yu. V. Tyutekin, Acoust. Phys. **51** (3), 347 (2005).
9. V. V. Tyutekin and A. I. Boiko, Acoust. Phys. **52** (3), 344 (2006).
10. Y. Tong, J. Fan, and B. Wang, J. Acoust. Soc. Am. **143** (6), 3332 (2018).
11. E. A. Skelton, J. Acoust. Soc. Am. **113** (1), 299 (2003).
12. S. D. Anderson, K. G. Sabra, M. E. Zakharia, and J. P. Sessarego, J. Acoust. Soc. Am. **131** (1), 164 (2012).
13. M. B. Salin, Acoust. Phys. **57** (5), 722 (2011).
14. J. P. Henderson, A. Plummer, and N. Johnston, Int. J. Hydromechatronics **1** (1), 47 (2018).
15. M. Rajabi, Acoust. Phys. **62** (3), 292 (2016).
16. M. Rajabi, Acoust. Phys. **62** (5), 523 (2016).
17. H. Überall, Acoust. Phys. **47** (2), 115 (2001).
18. P. Runkle and L. Carin, J. Acoust. Soc. Am. **106** (2), 605 (1999).